Supplementary Figure 1

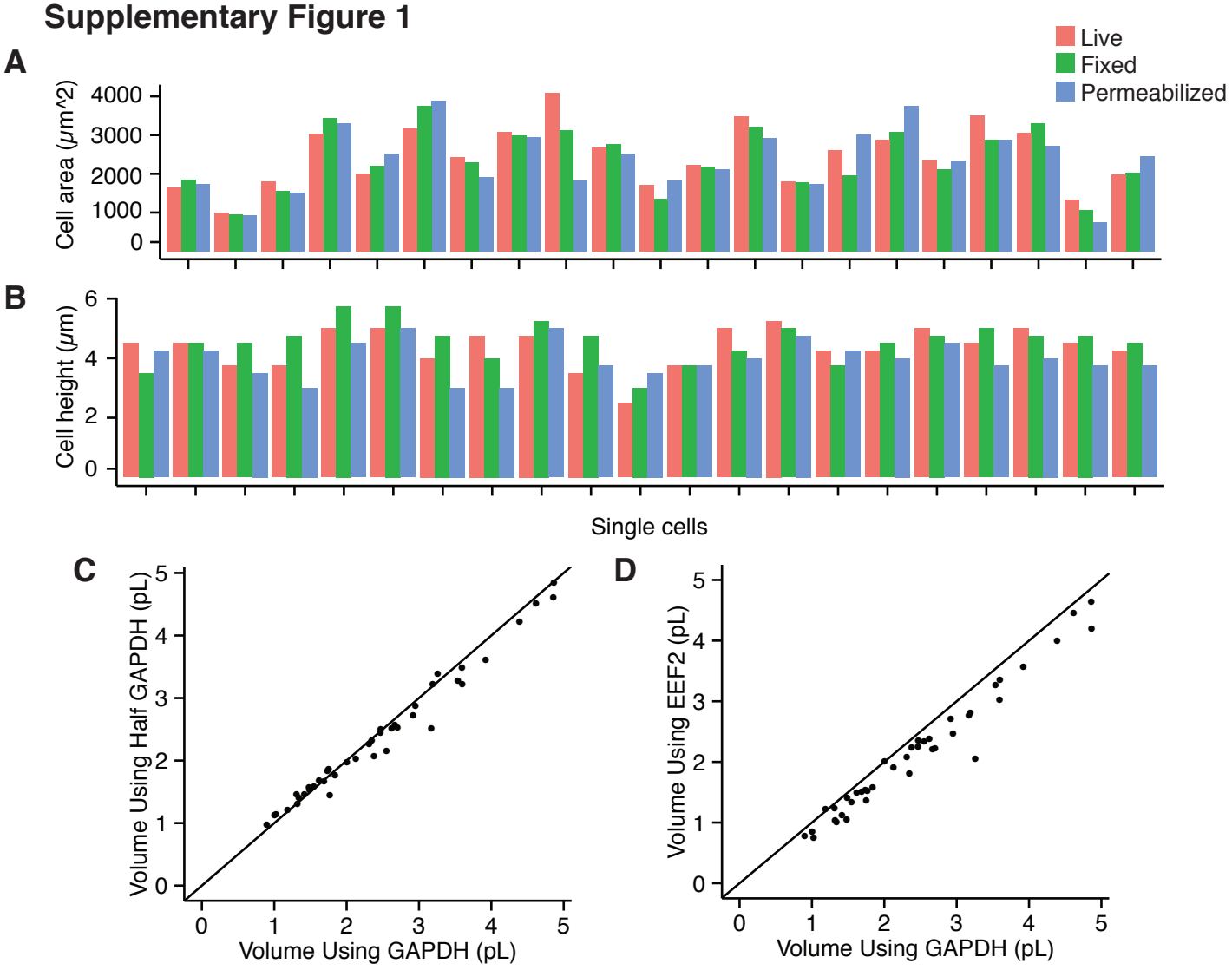

Supplementary Fig. 1. Controls for volume calculation.
A and B. We monitored cells on the microscope throughout the process of fixation. We took measurements of the same cells live, after fixing in 4% formaldehyde for 10 minutes, and after permeabilizing in ethanol for 30 minutes.
A. We measured the areas of the cells through brightfield images.
B. We measured the height of the cells by coating the cells with fluorescent beads.
These measurements indicate that the cells remain roughly the same size throughout the fixation and permeabilization process.
C. To demonstrate the robustness of the volume calculation algorithm, we calculated volume for the same cells using all the *GAPDH* mRNA spot coordinates as detected by RNA FISH, or using only half of the points, chosen randomly. Both methods result in approximately the same volume, suggesting that the number of points we use is sufficient to calculate the volume accurately.
D. We calculated volume using a different gene, *EEF2*. On average, *EEF2* has an abundance that is less than half that of *GAPDH* (mean EEF2 = 1079 mRNA/cell, mean *GAPDH* = 2673 mRNA/cell). Volume calculated using *EEF2* is systematically lower than that calculated using *GAPDH*, but the values are similar.
Black lines indicate a fit with intercept = 0 and slope = 1.

Supplementary Figure 2

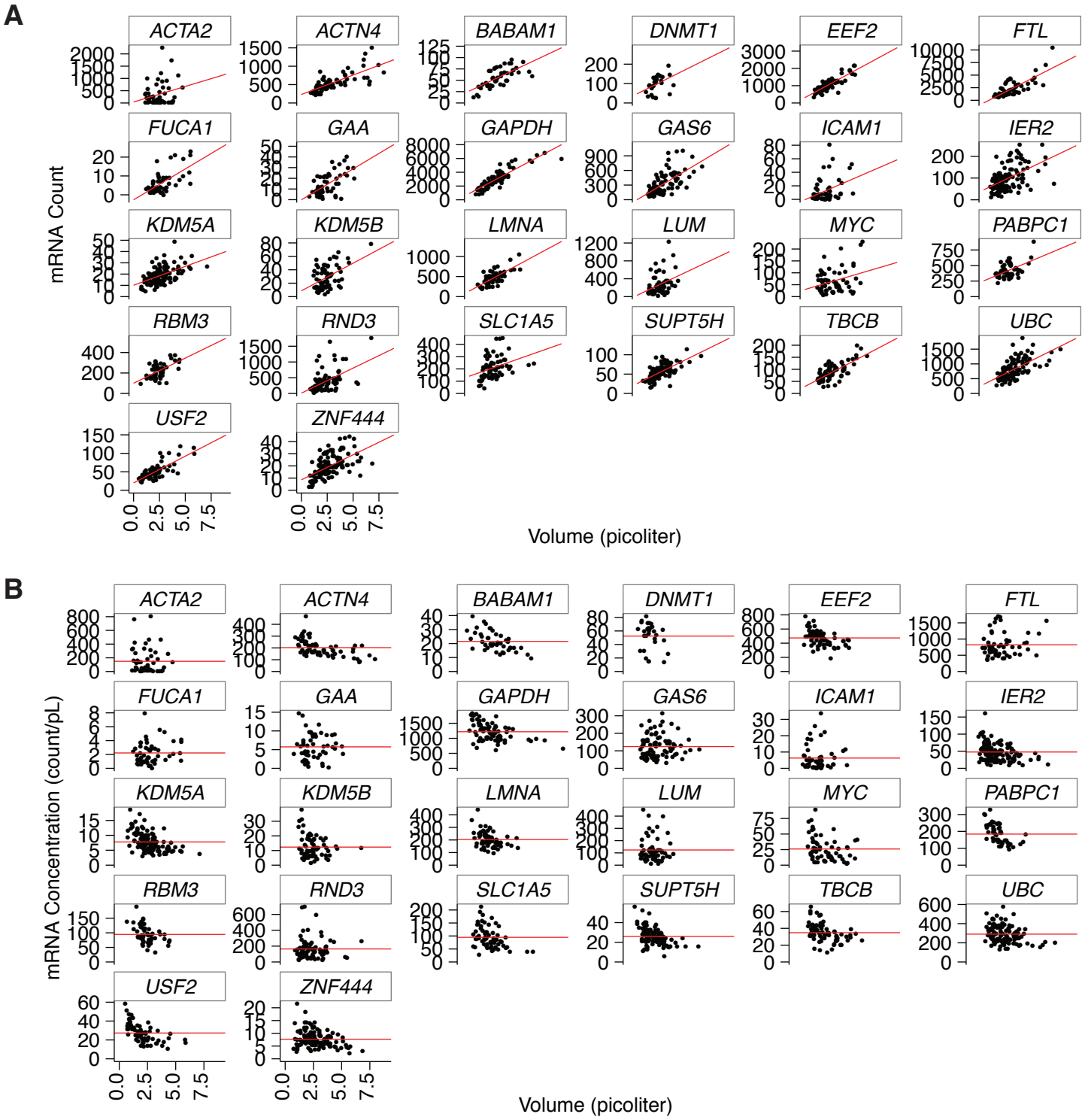

Supplementary Fig. 2. mRNA count (A) and concentration (B) measurements for all genes in cycling CRL2097 cells.

Each data point is an individual single cell measurement. In count plots, red line indicates best linear fit to the data. In concentration plots, red line indicates mean mRNA concentration. Each data set is a combination of at least two biological replicates.

Supplementary Figure 3

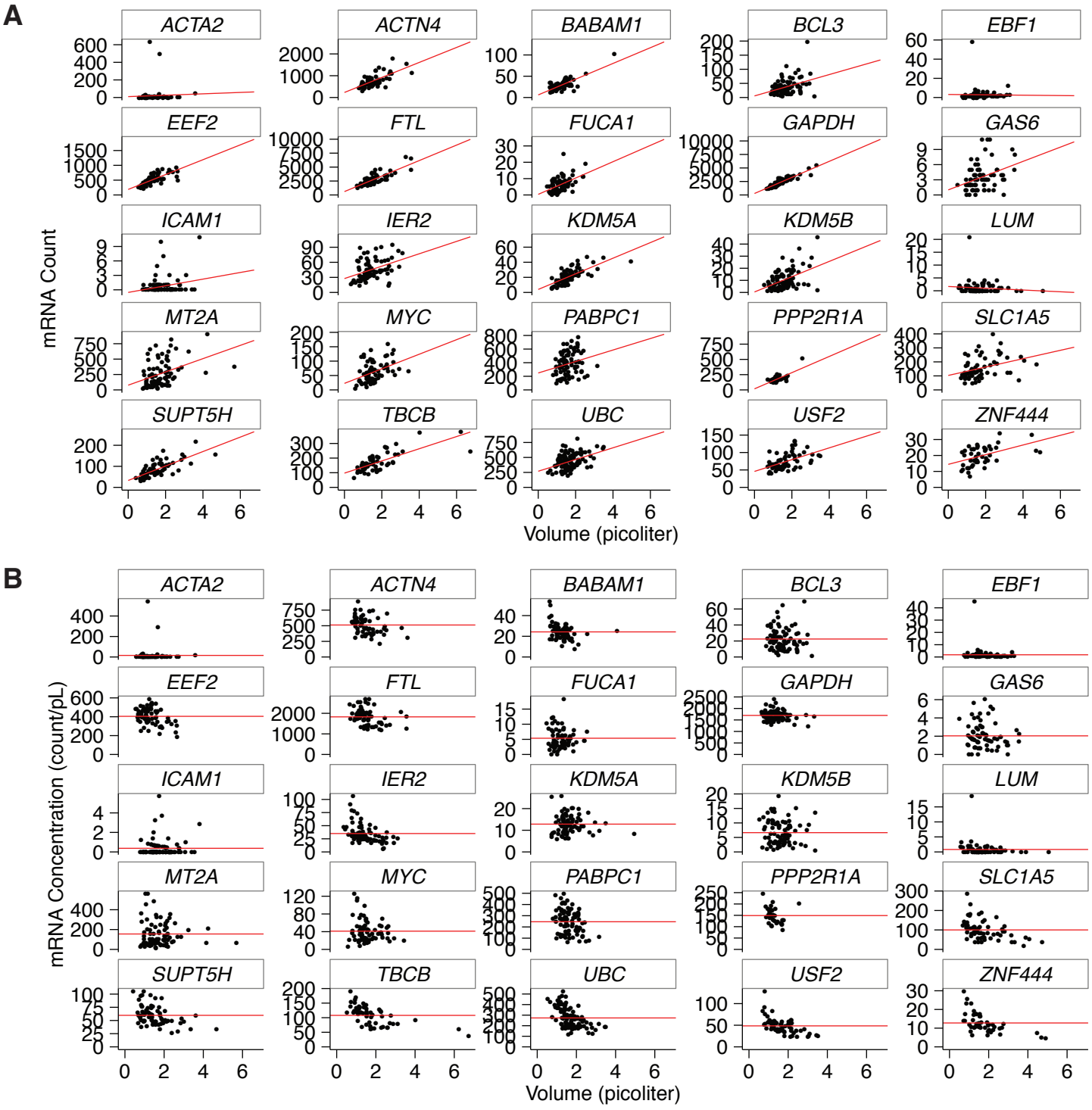

Supplementary Fig. 3. mRNA count (A) and concentration (B) measurements for all genes in cycling A549 cells.

Each data point is an individual single cell measurement. In count plots, red line indicates best linear fit to the data. In concentration plots, red line indicates mean mRNA concentration. Each data set is a combination of at least two biological replicates.

Supplementary Figure 4

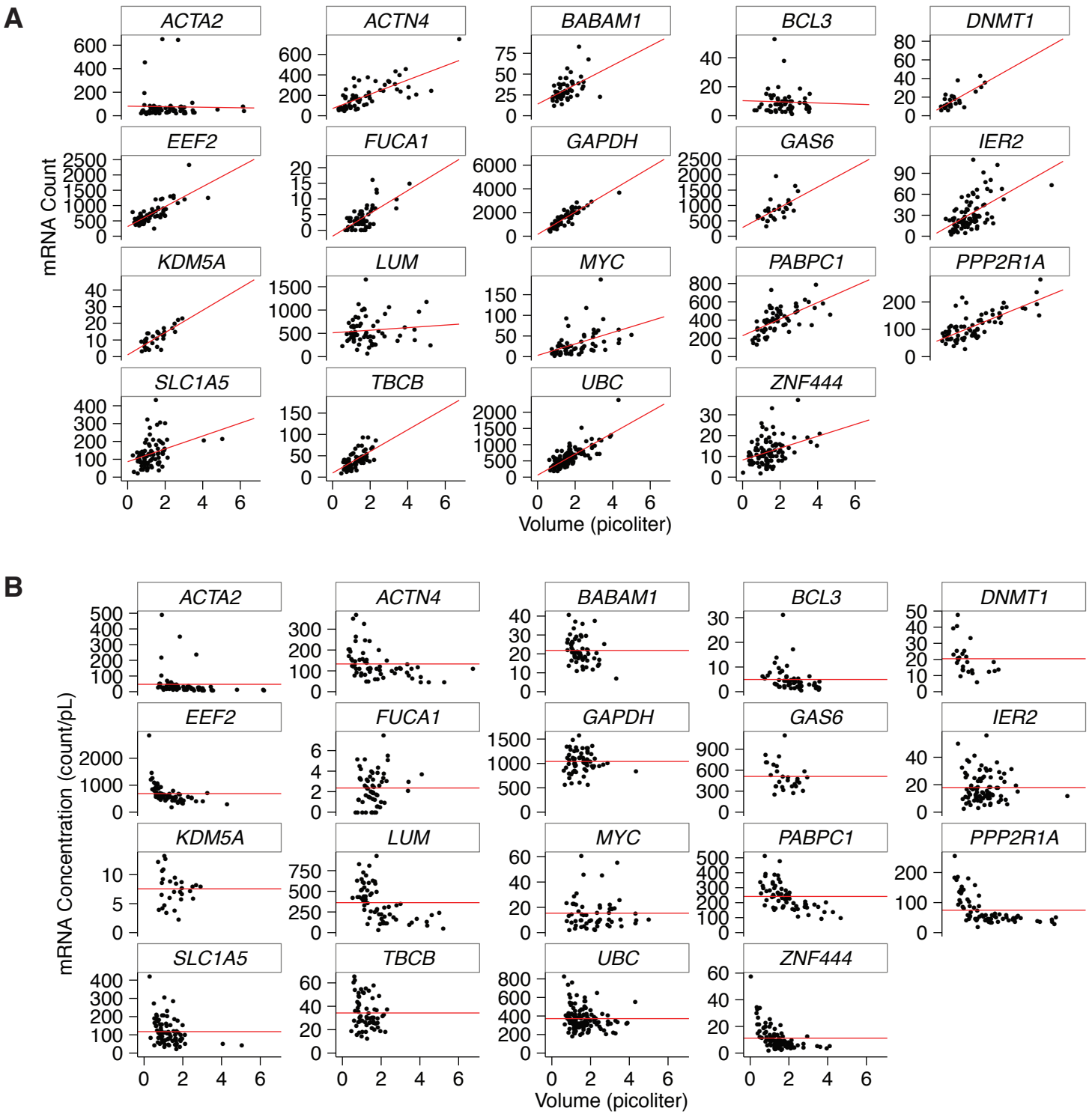

Supplementary Fig. 4. mRNA count (A) and concentration (B) measurements for all genes in quiescent CRL2097 cells.

Each data point is an individual single cell measurement. In count plots, red line indicates best linear fit to the data. In concentration plots, red line indicates mean mRNA concentration. Each data set is a combination of at least two biological replicates.

Supplementary Figure 5

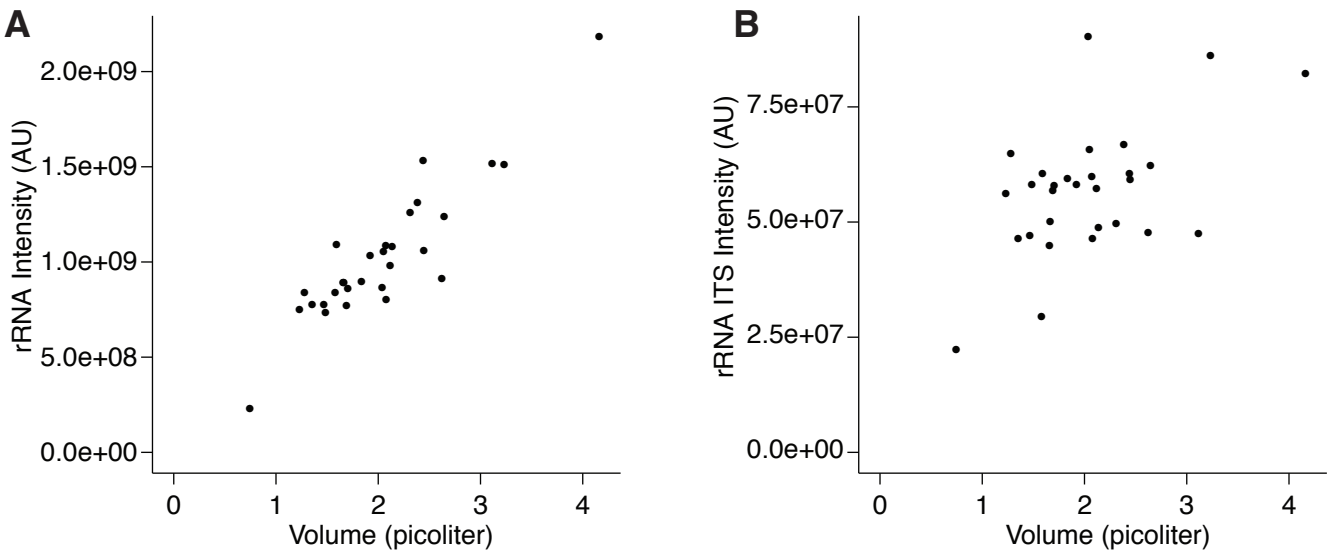

Supplementary Fig. 5. Ribosomal RNA.
A. We measured ribosomal RNA by quantifying total fluorescence intensity in the cytoplasm from an rRNA FISH probe in cycling CRL2097 cells.
B. We measured the rRNA ITS (the rRNA "intron") by quantifying total fluorescence intensity in the nucleus from an ITS RNA FISH probe.
rRNA and the rRNA ITS both scale with volume to some degree, suggesting that the production of ribosomal RNA scales with volume. We have shown that mRNA scales with volume, so a similar scaling of rRNA is not inconsistent with the production of protein to scale with volume as well. The data shown is one of three biological replicates.

Supplementary Figure 6

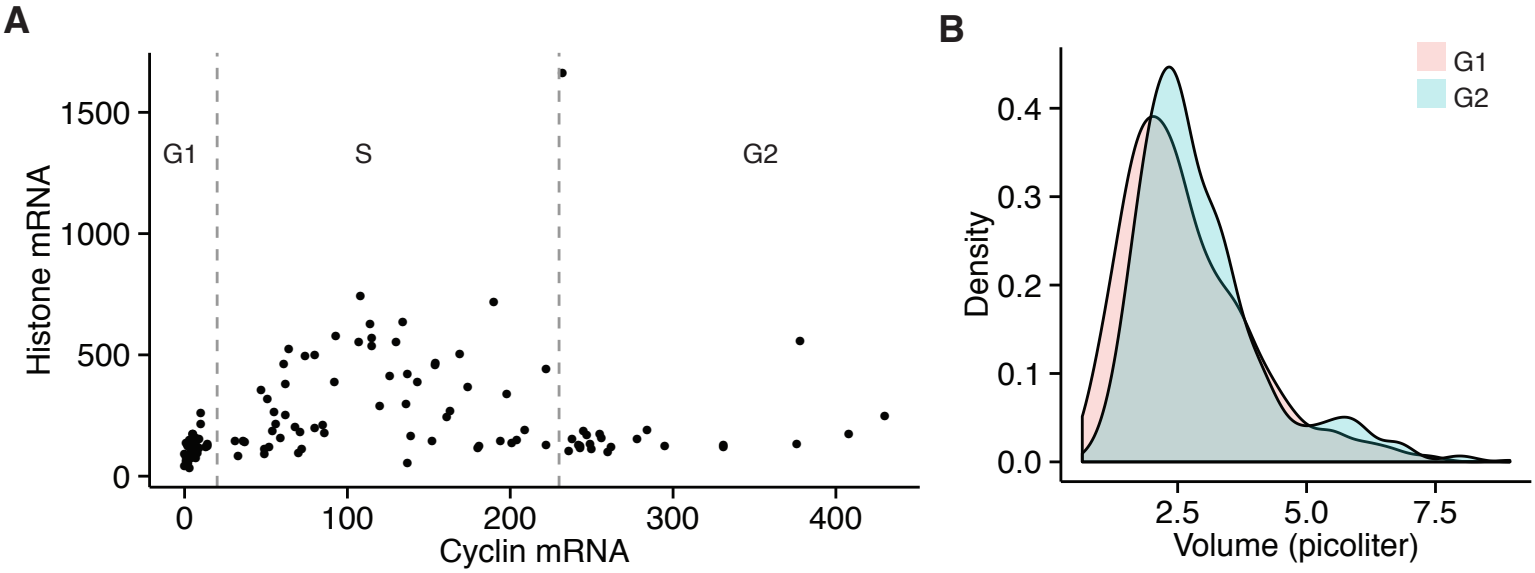

Supplementary Fig. 6. Cell cycle characterization.
A. We simultaneously measured *CCNA2* and *HIST1H4E* mRNA by RNA FISH to precisely determine cell cycle position. Each data point is a single cell measurement. *CCNA2* is highly expressed in S and G2, but not G1. *HIST1H4E* is highly expressed only in S phase. Cells with low *CCNA2* and *HIST1H4E* are in G1 (cutoff = 20 *CCNA2* mRNA), cells with mid-range *CCNA2* and high *HIST1H4E* are in S, and cells with high *CCNA2* and low *HIST1H4E* are in G2 (cutoff = 230 *CCNA2* mRNA). We determined thresholds for all samples using this method. Data shown are from one of four biological replicates.
B. Volume distributions in G1 and G2. We determine cell cycle position using *CCNA2*. We note that G2 cells are larger than G1 cells, but only 10% larger on average, possibly due to non-linearities in growth over the course of the cell cycle. n = 841 cells in G1, 191 cells in G2.

Supplementary Figure 7

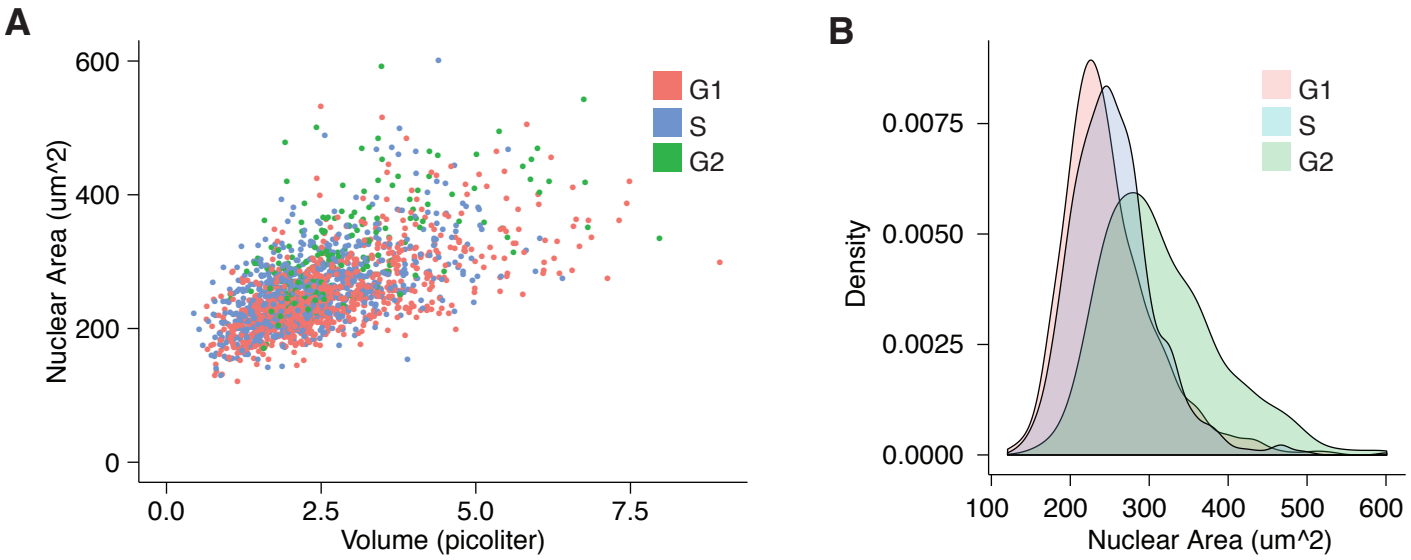

Supplementary Fig. 7. Nuclear area scales with cell cycle stage and cell size.
A. Nuclear area vs. cytoplasmic volume. We measure cytoplasmic volume using our standard method. We measure nuclear area using the DAPI stain. We note that we only measure nuclear area and not volume.
B. Density plot of nuclear area across cell cycle stages.
While nuclear area generally scales with cytoplasmic volume, there is considerable spread in the data (R^2 = 0.358). n = 1866 cells.

Supplementary Figure 8

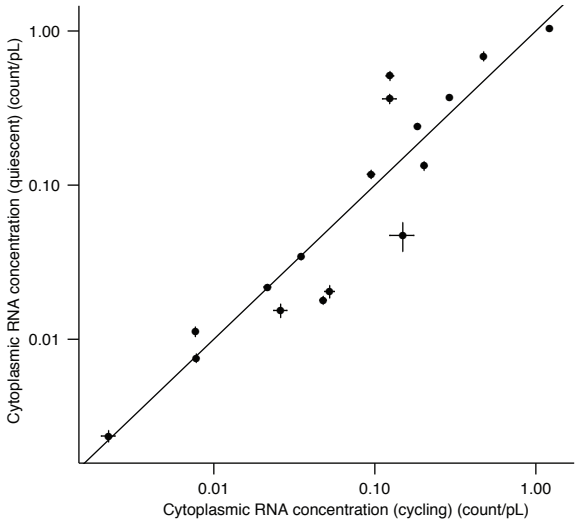

Supplementary Fig. 8. mRNA concentration is similar for cycling and quiescent cells.
We calculated the average mRNA concentration for 17 genes in both the cycling and quiescent state in human foreskin fibroblast cells. Each data point represents one gene. Each gene had a minimum of 2 biological replicates, with at least thirty cells per replicate. Line has intercept 0 and slope 1. Error bars represent standard error.

Supplementary Figure 9

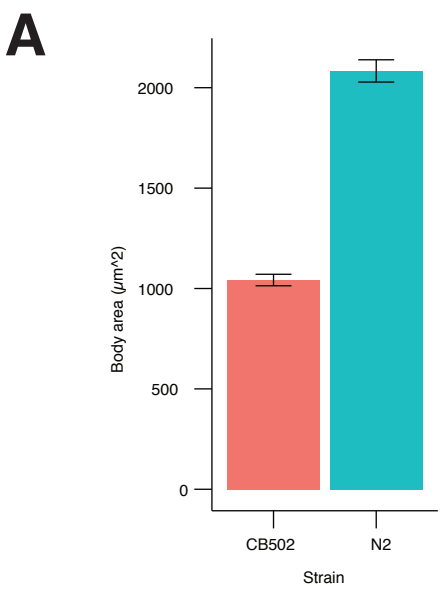

Supplementary Fig. 9. Comparison of size between CB502 and N2 strains.
A. CB502 worms are smaller by ~50%. We obtained these data by identifying the outline of the worm through transmitted light illumination and calculating the area of each worm. All error bars represent SEM.

Supplementary Figure 10

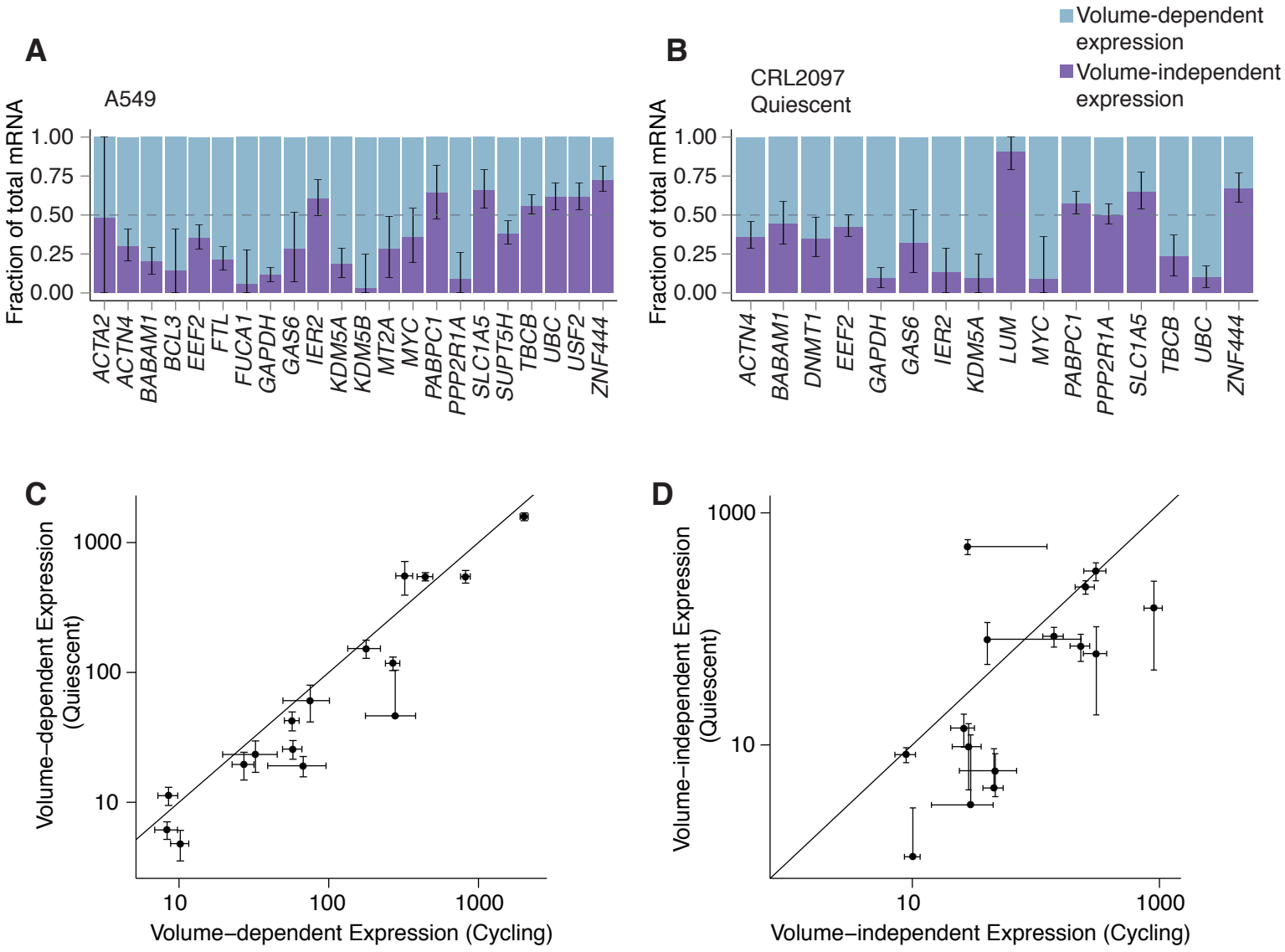

Supplementary Fig. 10. Volume-dependent and -independent expression in all cell types and growth conditions.

We calculated the fraction of volume-dependent and -independent transcription for all genes using the best-fit line for each gene and the average volume for each cell type or condition, as in Fig. 1. We calculated this for A. cycling A549 cells and B. quiescent CRL2097 cells.

C,D. We compared volume-dependent and -independent abundance for cycling and quiescent cells. Both volume-independent and volume-dependent expression are lower in quiescent cells.

All error bars represent confidence intervals of the slope or intercept of the fit, normalized to the scale of the plot. In C and D, we omitted error bars that extended below zero.

Each gene had a minimum of two biological replicates, with at least 30 cells per replicate. We omitted highly variable genes with intercept terms less than zero.

Supplementary Figure 11

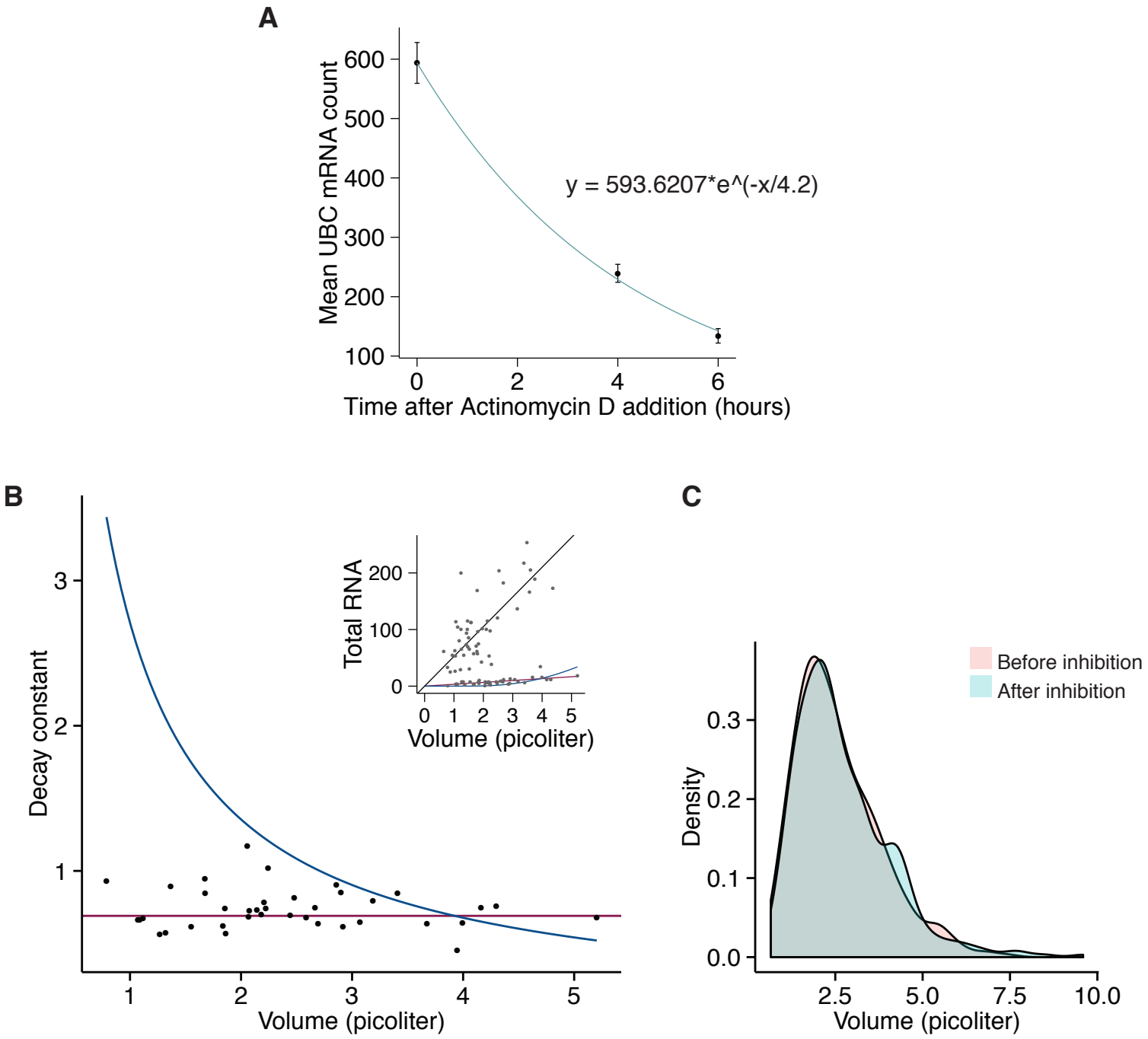

Supplementary Fig. 11. Actinomycin D transcription inhibition controls.
A. RNA degrades exponentially when transcription is inhibited with Actinomycin D. Pictured is UBC mRNA 0,4, and 6 hours after transcription block.
B. Degradation experiment with *IER2*. We inhibited transcription in CRL2097 cells using Actinomycin D for 4 hours and allowed RNA to degrade. Inset shows *IER2* before and after inhibition. Each point represents a single-cell measurement. We calculated the decay constant for each cell using the best-fit line before inhibition (see Methods). Blue line shows fit if degradation were volume-dependent; red line shows fit if transcription were volume-dependent. Data represent one of three biological replicates
C. Distribution of cell volumes before and after inhibition by Actinomycin D. The volume distribution is the same before and after we inhibit transcription. Although we cannot track a single cell before and after inhibition, this suggests that Actinomycin D likely does not change the volume of a cell, so it is appropriate to use the fit line before inhibition to calculate the decay constant. n = 459 cells before inhibition, 413 cells after inhibition.

Supplementary Figure 12

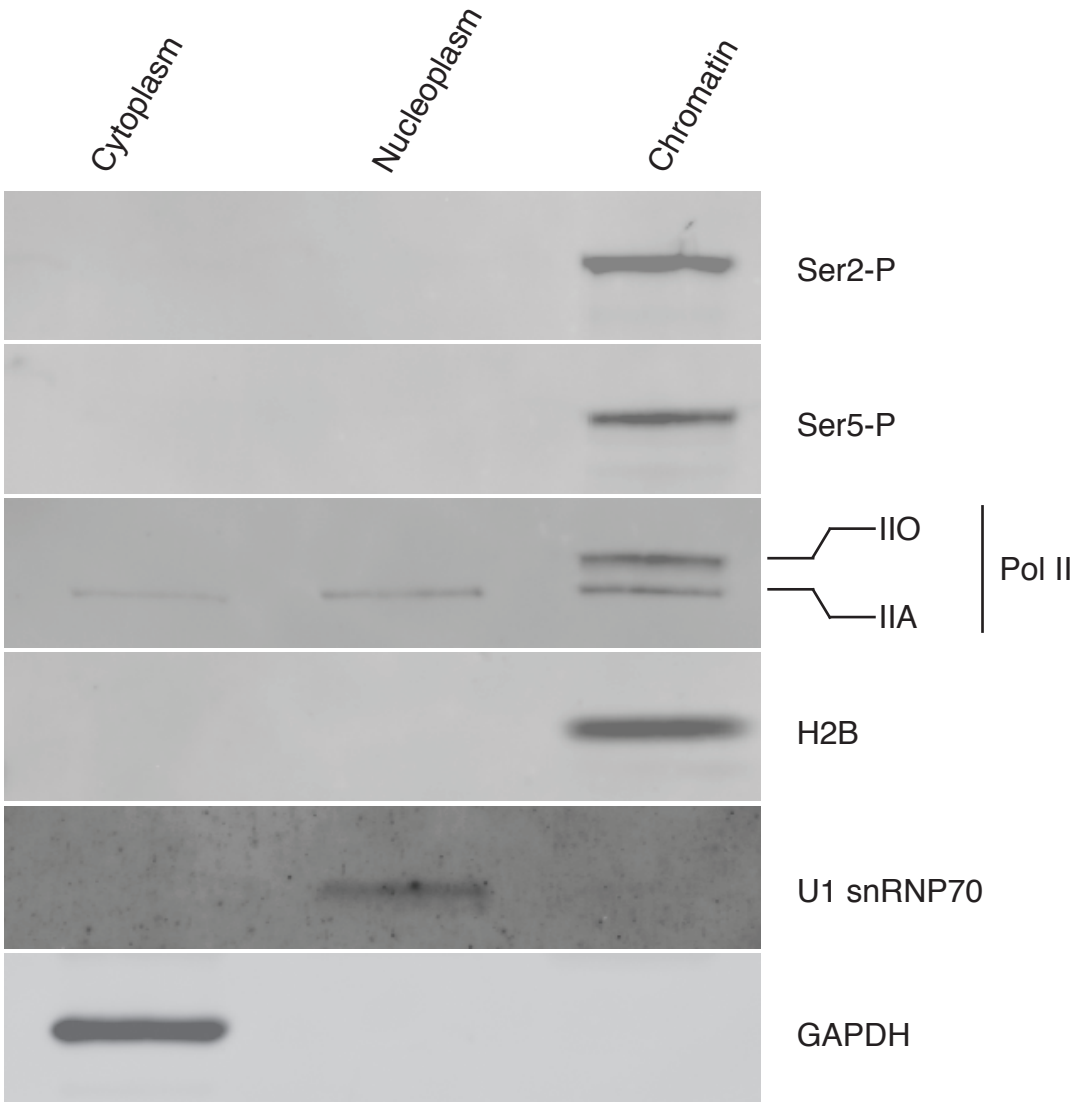

Supplementary Fig. 12. RNA Polymerase II fractionation.
Western blot analysis shows the efficient separation of cell fractions and reveals that ≥99% of elongating Pol II (C-terminal domain (CTD) Ser2- and Ser5-phosphorylated forms, and the general CTD hyper-phosphorylated form (IIO) of Pol II) is captured in the chromatin fraction. We also probed proteins with defined subcellular localization (Chromatin marker, Histone 2B; nucleoplasm marker, U1 snRNP70; cytoplasm marker, GAPDH). Data is from a representative Western blot experiment, using subcellular lysates generated from the same batch of CRL2097 cells. Sample volumes have been adjusted so that Western blot signals of the subcellular fractions can be compared. Further details are given in the Methods section.

Supplementary Figure 13

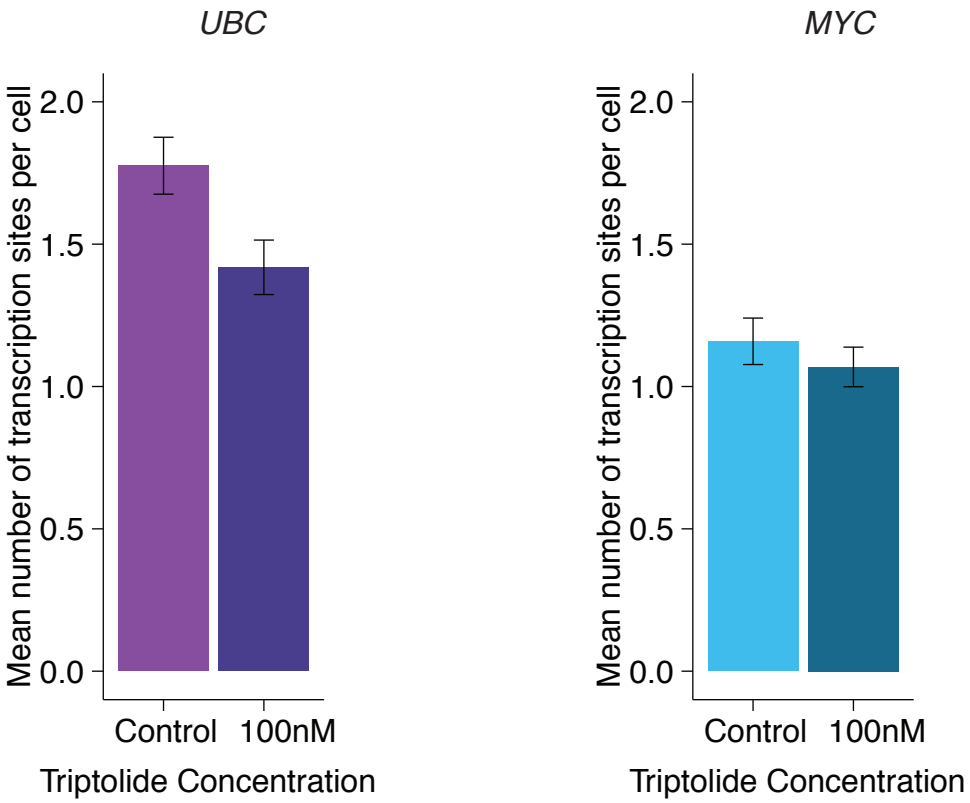

Supplementary Fig. 13. Treatment with triptolide has a small effect on transcriptional frequency. We treated CRL2097 cells with 100nM triptolide (100nM) or simply replaced the media on cells (Control) and fixed in methanol after one hour. For genes *UBC* and *MYC*, we identified active transcription sites through intron/exon colocalization and quantified the number of active transcription sites per cell with and without triptolide. Bars represent mean of cells, error bars are SEM. The data shown here is from two replicates, for a total of 282 cells for *UBC* and 257 cells for *MYC*. For both genes, the change in frequency between conditions is small compared to the change in intensity (Fig. 4).

Supplementary Figure 14

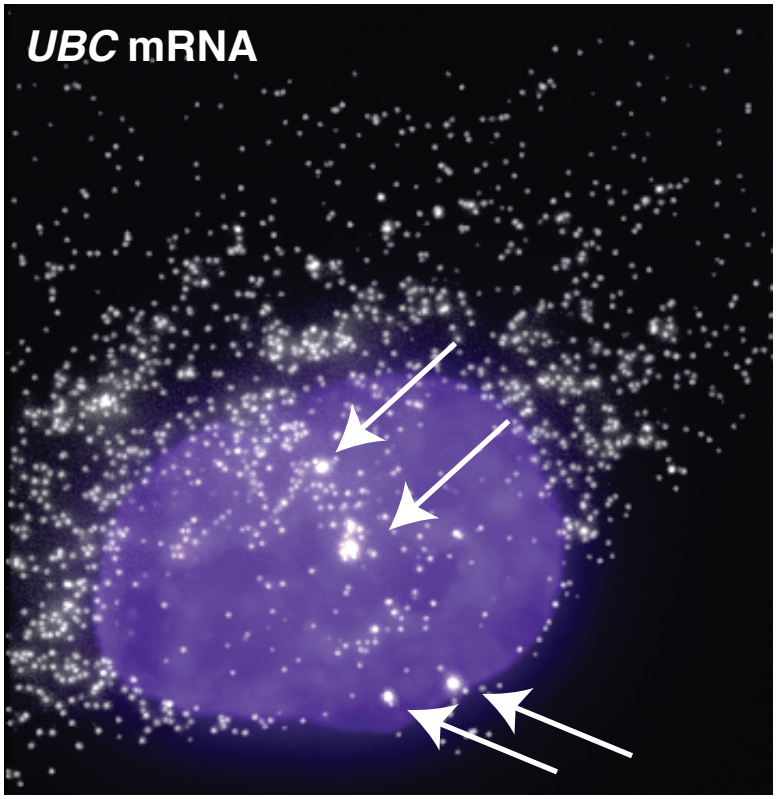

Supplementary Fig. 14. Replicated gene copies are transcriptionally competent.
UBC mRNA in a CRL2097 cell. RNA FISH probe in white, DAPI stain in purple. White arrows indicate transcription sites. We detect transcription sites through intron/exon colocalization by RNA FISH. This cell is in G2 and has four transcription sites, demonstrating that all gene copies are transcriptionally competent after replication.

Supplementary Figure 15

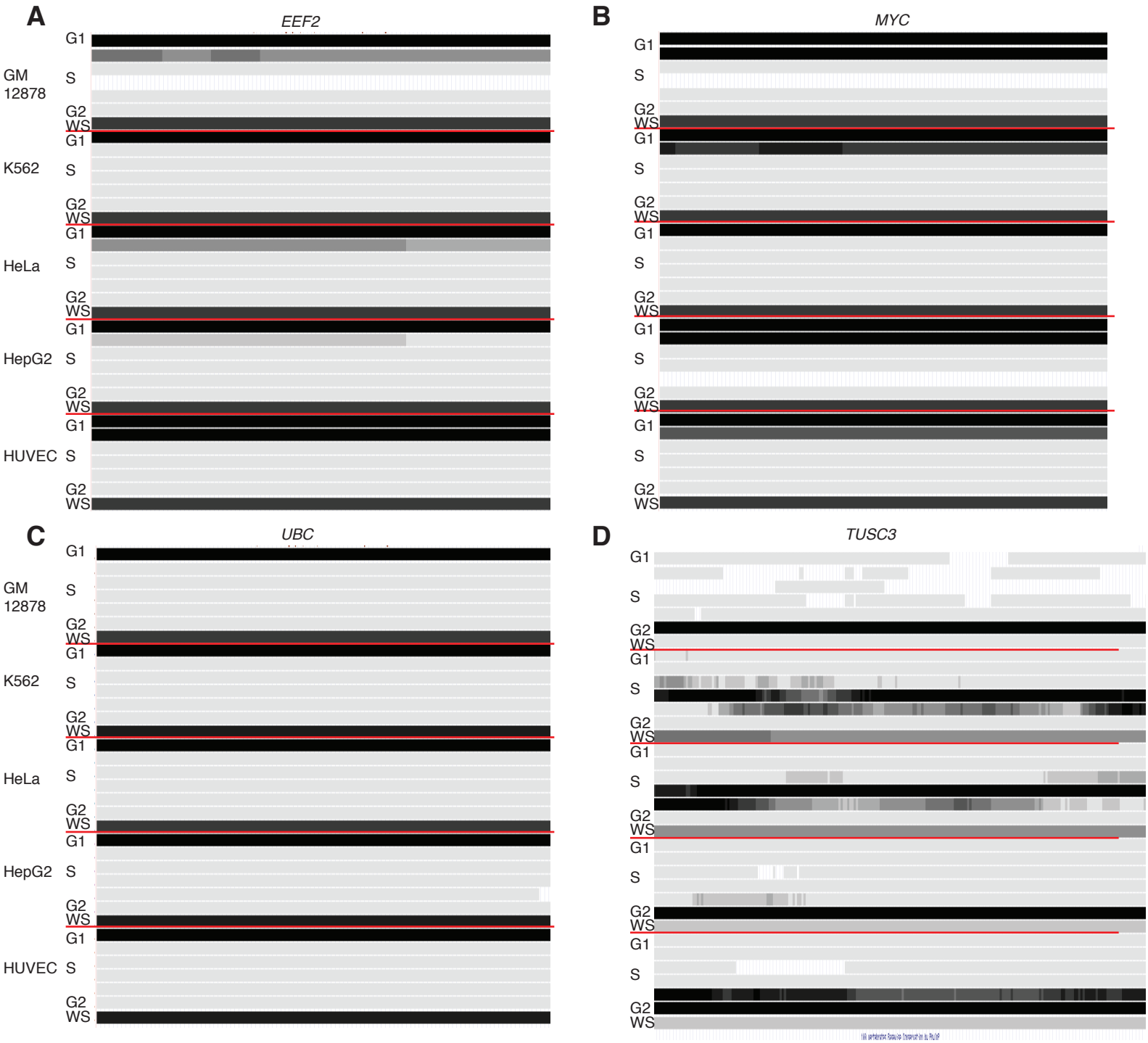

Supplementary Fig. 15. *EEF2*, *MYC*, and *UBC* genes are replicated early in the cell cycle; *TUSC3* replicates late.

A-D. Tracks from UCSC genome browser displaying UW Repli-Seq data in GM12878 (lymphoblastoid), K562 (chronic myelogenous leukemia), HeLa (cervical cancer), HepG2 (liver carcinoma), and HUVEC (human umbilical vein endothelial) cell lines. The track displays data for different points in the cell cycle: G1, S1 (early S phase), S2 (middle-early S phase), S3 (middle-late S phase), S4 (late S phase), and G2. WS represents a wavelet-smoothed transform of the six other tracks. This data was generated by sequencing newly-replicated DNA in each point in the cell cycle. Darkness of track corresponds to read density. Each track shown corresponds to entire length of each gene. Data is shown for:

A. *EEF2*, an early replicating gene, B. *MYC*, another early replicating gene, C. *UBC*, another early replicating gene, and D. *TUSC3*, a late replicating gene.

Supplementary Figure 16

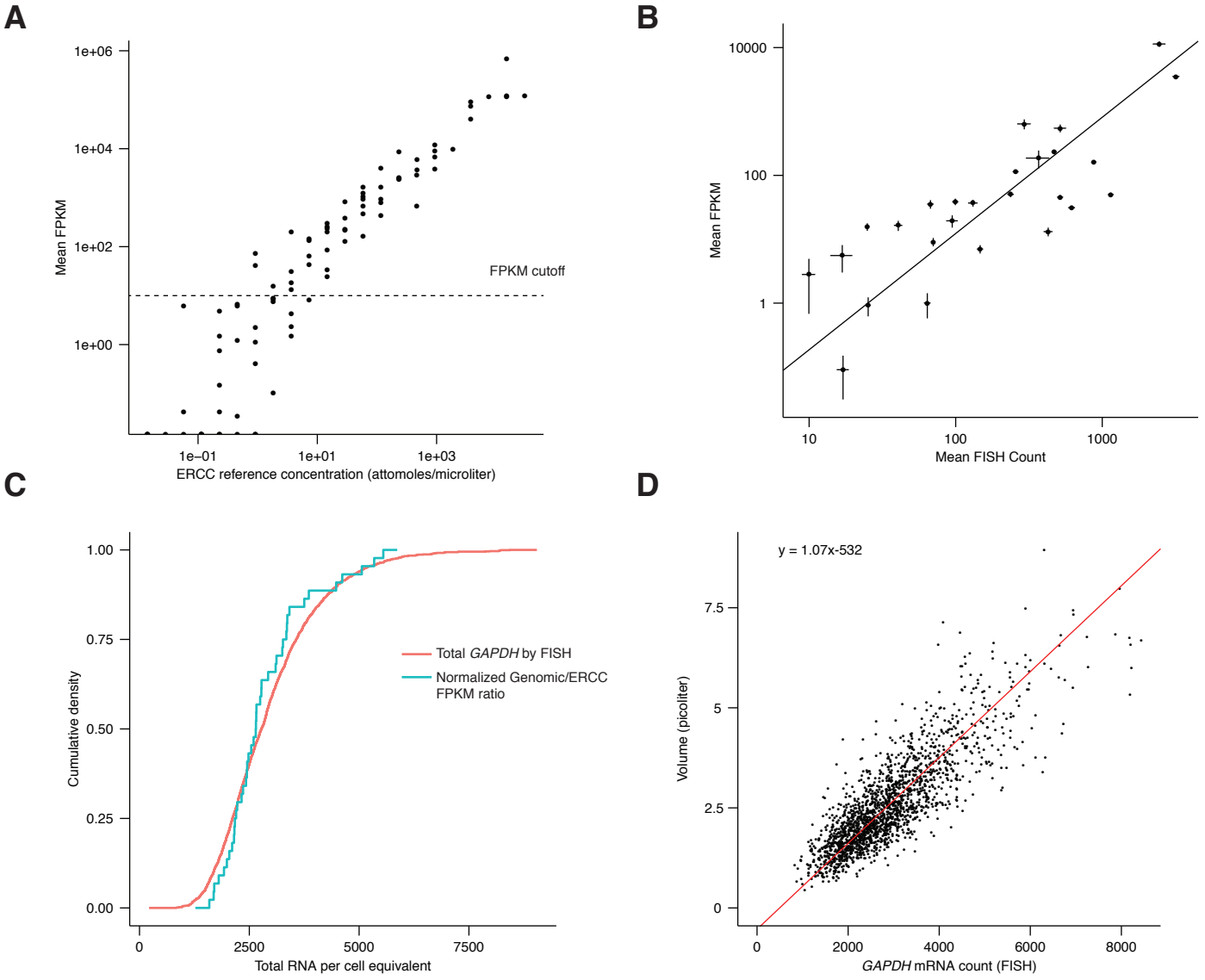

Supplementary Fig. 16. Calibration of single-cell sequencing data.

A. Mean FPKM and known concentrations for each of the ERCC reference transcripts. Each point represents a single ERCC transcript and is an average over all 96 samples. Below 10 FPKM, we begin to see significant dropouts, and therefore choose and FPKM of 10 as our cutoff for “reliable” measurements. All other data in the manuscript is taken from genes having greater than 10 FPKM.

B. Mean count as measured by RNA FISH vs. mean FPKM from single-cell RNA sequencing. Each point represents a single gene and is an average over 44 single cells for single-cell sequencing, and an average over at least two biological replicates with at least 30 cells apiece for RNA FISH. These data suggest that an FPKM of 1 corresponds to approximately 23.2 transcripts per cell, as measured by RNA FISH in our cells, although the relationship between RNA FISH counts and FPKM scales nonlinearly (FPKM ~ (FISH)1.7, see Methods). We used this fitted relationship between RNA FISH count and FPKM to transform FPKM into transcript counts. Error bars represent SEM.

C. Comparison of “total RNA” distributions from single-cell sequencing and RNA FISH. Data represent a collection of total RNA measurements from single cells. We assume that total GAPDH mRNA counts by RNA FISH are proportional to total RNA. For sequencing data, we use the ratio of reads mapped to genomic loci to reads mapped to ERCCs as a proxy for total RNA. We scaled this ratio to have the same mean as the distribution of total RNA by RNA FISH. After scaling, the distributions are similar, suggesting that our method for measuring total RNA via the ratio of genomic to ERCC transcripts is sound.

D. Mapping between total RNA count (here, total GAPDH mRNA in single cells) and volume, as measured by RNA FISH. Each point represents a single cell. We use this mapping to convert total RNA from sequencing experiments to actual volume. The red line is the best fit, as computed by principle components analysis.

Supplementary Figure 17

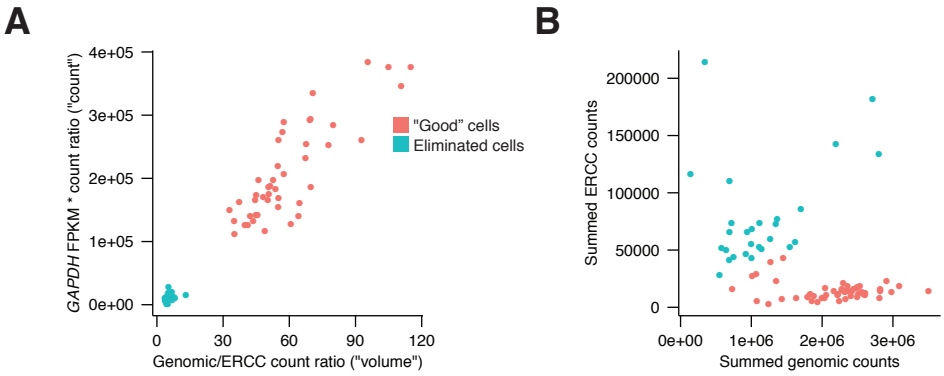

Supplementary Fig. 17. Classification of cells to eliminate from sequencing analysis.
A. “Count” vs. “volume” for GAPDH from single-cell sequencing data. We define “volume” as the ratio between genomic reads and ERCC reads for each cell. This quantity is more representative of total RNA, which we know to be roughly proportional to volume, although the relationship is not exactly proportional due to volume-independent transcription (see Supplementary Fig. 10). We observed two clearly distinct classes of cells, those with a volume range that matches what we see by imaging and RNA FISH and those that have very low volumes. For unknown reasons, these cells ended up with a considerably higher ratio of ERCC reads than genomic reads, and we eliminated them from our subsequent analyses.
B. ERCC counts vs. genomic counts for the cells that we kept and those we eliminated.

Supplementary Figure 18

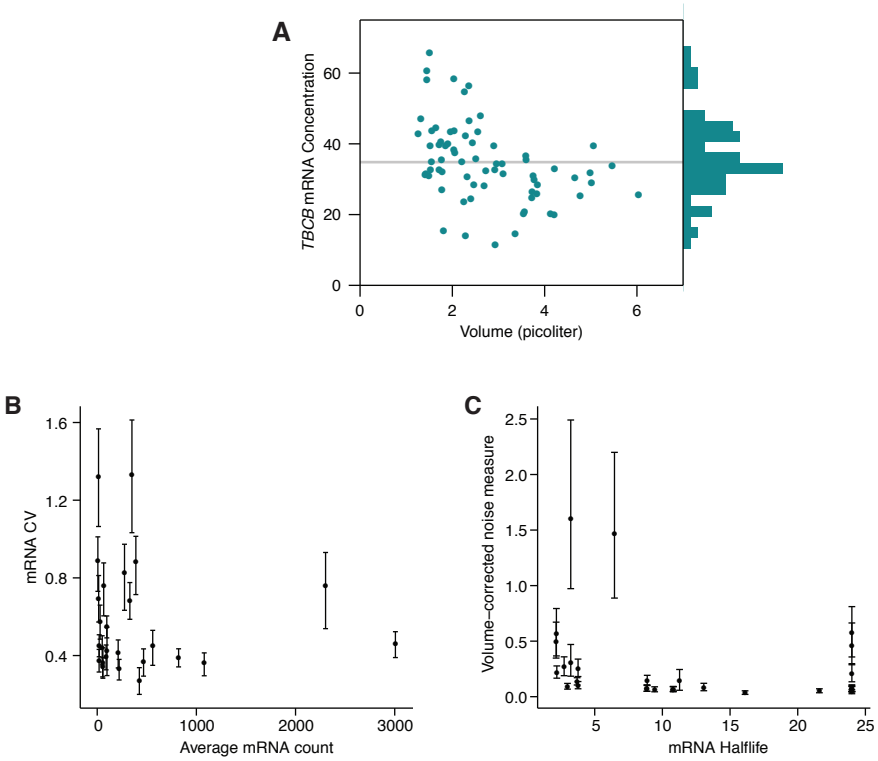

Supplementary Fig. 18. Quantification of cell-to-cell variability in gene expression.
A. *TBCB* mRNA concentration vs. volume. These data are the same as in (Fig. 6C), but each is normalized by volume. Histogram indicates distribution of mRNA concentration. Gray line indicates average concentration. Data are from a combination of two biological replicates.
B. We calculated the coefficient of variation (CV = standard deviation / mean) for mRNA counts in single human foreskin fibroblast cells and plotted against mean RNA count measured by RNA FISH. We find that CV does not scale with mean mRNA abundance.
C. We compared volume-corrected noise measure and mRNA half-life. We obtained half-life values from Tani et al., Genome Res. (2012). We find that volume-corrected noise measure does not depend strongly on half-life.
(B,C) Each data point represents one gene. For each gene, we have at least two biological replicates with at least 30 cells per replicate. Error bars represent 95% confidence intervals, calculated by bootstrapping.

Supplementary Figure 19

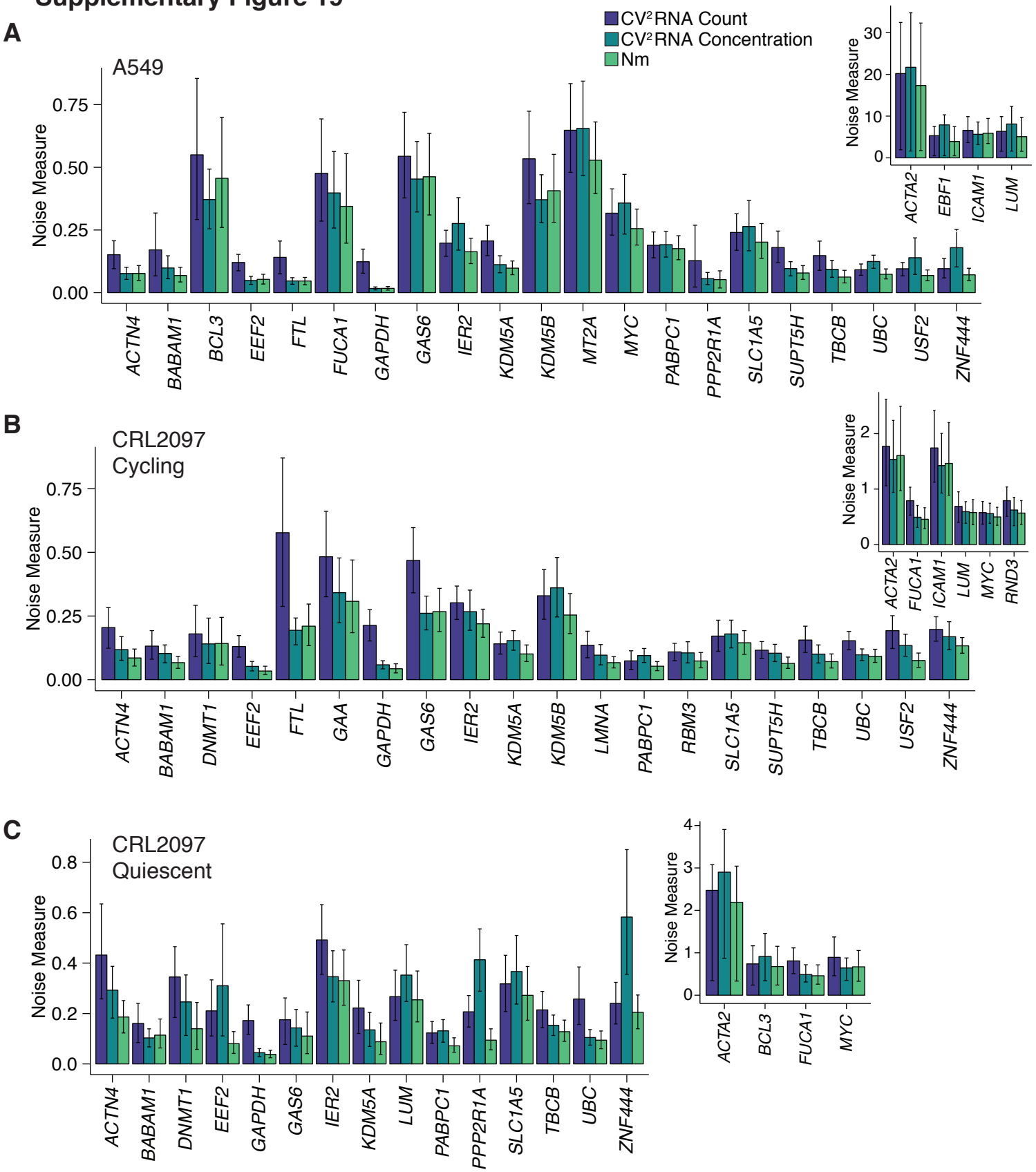

Supplementary Fig. 19. Comparison of mRNA CV, concentration CV, and volume-adjusted CV for all cell types and growth conditions.

A-C. mRNA CV, concentration CV, and volume-adjusted CV for: A. Cycling A549 cells, B. Cycling CRL2097 cells, C. Quiescent CRL2097 cells. Insets show genes that exhibit higher cell-to-cell variability, and had values too high for main axes. Generally, mRNA CV is highest, followed by concentration CV and volume-adjusted CV. Error bars represent 95% confidence intervals by bootstrapping.

Supplementary Figure 20

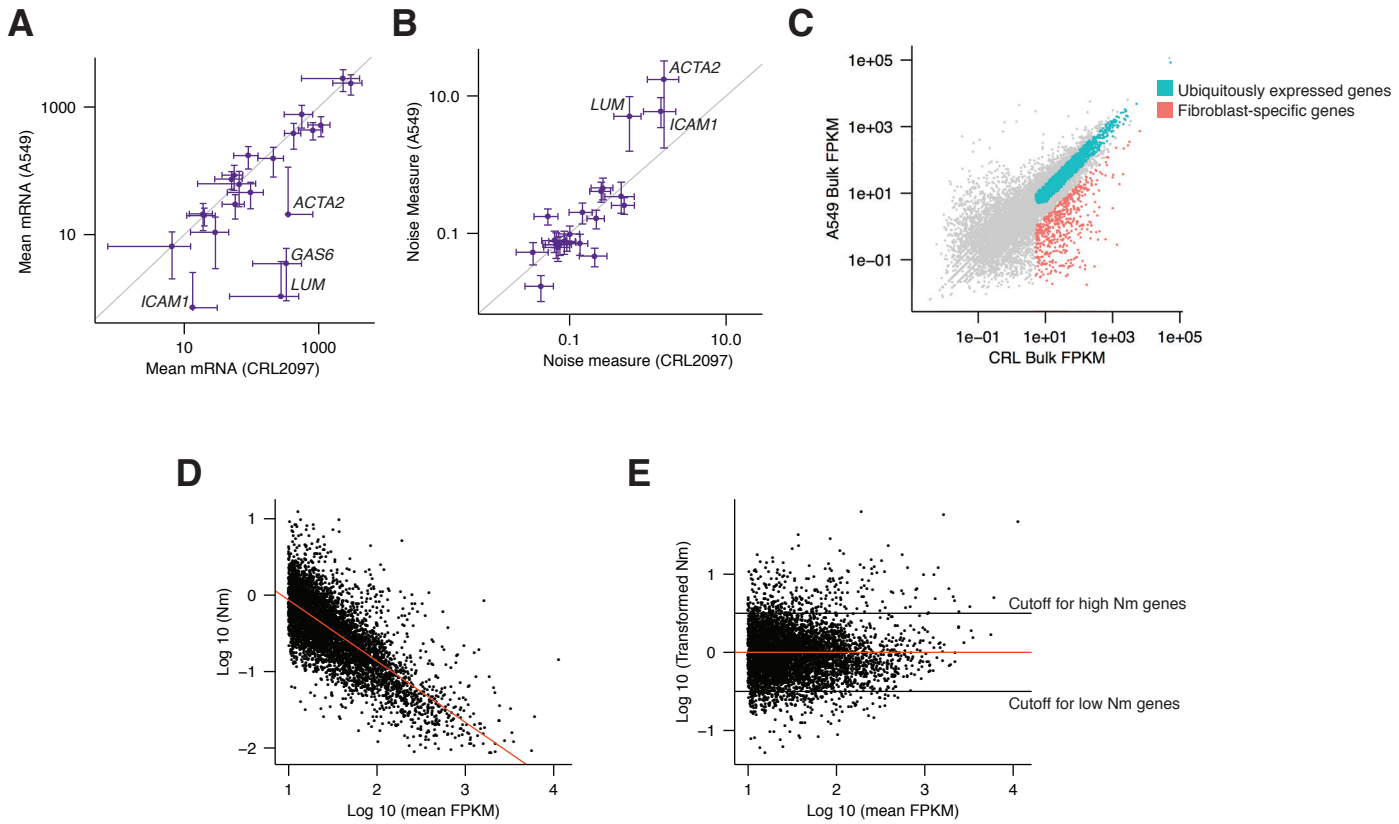

Supplementary Fig. 20. Classification of noise level and cell type specificity.
A. Average mRNA counts in cycling hFF and A549 cells. Gray line indicates a 1:1 correspondence. Error bars represent standard error of the mean.
B. Volume-corrected noise measure in cycling hFF and A549 cells. Gray line indicates a 1:1 correspondence. Nm calculated by bootstrapping; error bars represent 95% confidence interval. Data for each gene is a combination of at least two biological replicates, with at least 30 cells per replicate.
C. FPKM measurements from bulk RNA-sequencing in hFF and A549 cells. Each point represents one gene. We classified genes as "ubiquitously expressed" if they had >5 FPKM in both cell types and differed by less than a factor of 2 in FPKM across the two cell types. We considered genes "fibroblast specific" if they had >5 FPKM in fibroblasts and their FPKM was greater than five times higher in fibroblasts that A549 cells.
D. Single-cell RNA-sequencing data in hFF cells. Each point represents one gene. We used the method described in Supplementary Fig. 14 and Methods to calculate Nm for each gene. We observe that higher abundance genes typically have lower Nm values. Red line indicates best fit line.
E. The same data as in D, but transformed to remove the volume-dependence from Nm. Red line here is the transformed fit line from D. We use this transformed data to select volume-matched "low Nm" and "high Nm" genes using a cutoff of Nm=0.5 and Nm=-0.5, respectively. We selected 307 high Nm genes and 257 low Nm genes. Note that these high Nm genes actually have a higher mean abundance (FPKM=196.5) than the low Nm genes (FPKM=55.4), thus showing that the observed differences in noise levels are not due to the overall increase in noise in genes of low abundance.

Supplementary Figure 21

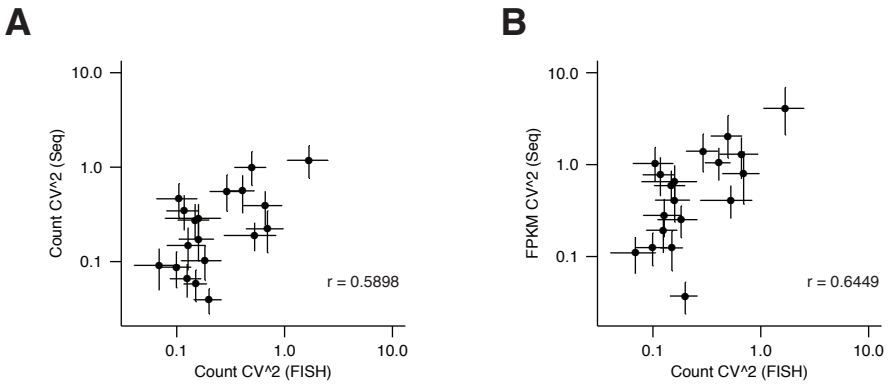

Supplementary Fig. 21. Comparison of noise metrics through RNA FISH and single-cell sequencing.
A. Correspondence between CV^2 of RNA FISH counts and CV^2 of inferred counts from single-cell sequencing (transforming FPKM as in Supplementary Fig. 14 and Methods). Each data point represents a single gene.
B. Same as A, except using CV^2 of FPKM from single-cell sequencing instead. Correlation is slightly higher than in A.
For all plots, Nm is calculated by bootstrapping; error bars represent 95% confidence intervals, calculated by bootstrapping.